UDC 621.793.18.06

NUMERICAL SIMULATION AND EXPERIMENTAL INVESTIGATION OF REMELTING PROCESSES

A. JARDY
Institut Jean Lamour (UMR CNRS – Universite de Lorraine 7198) Parc de Saurupt, CS 50840, F-54011 Nancy Cedex, France Laboratoire d'Excellence DAMAS, France. E-mail: alain.jardy@univ-lorraine.fr

The numerical simulation of remelting processes enables us to link the local solidification conditions to the operating parameters. Here, we discuss some recent studies aiming to develop specific aspects, e.g. the alternating current distribution during ESR of steels and superalloys, the ensemble arc motion in a VAR furnace and the influence of electromagnetic stirring on the macrosegregation in remelted ingots. 27 Ref., 1 Tabl., 5 Figures.

Key words: vacuum arc remelting, numerical simulation, electromagnetic stirring, current distribution, macrosegregation

I. Introduction

Consumable electrode remelting processes have been developed to produce high-performance alloys dedicated to critical applications, for which high metallurgical quality ingots are necessary. Consequently, primary melting is not sufficient and remelting provides valuable advantages such as a fine grain structure, limited occurrence of solidification defects, low level of micro- and macrosegregation and good soundness of ingots.

The principle of the VAR (Vacuum Arc Remelting) process, as illustrated in figure 1-a, consists in melting a consumable metallic electrode of the required grade under a high vacuum, in order to obtain a sound ingot of good structural quality [1]. During remelting, an electric arc is maintained between the tip of the electrode (which acts as the cathode) and the top of the secondary ingot, in order to ensure melting of the electrode. Liquid metal falls through the arc plasma and progressively builds up the ingot, which solidifies in contact with a water-cooled copper crucible. In order to stabilize the arc, it can be confined with the aid of an axial magnetic field created by an external induction coil. The interaction with the melting current stirs the liquid metal, the rotation induced being in the orthoradial direction. By reversing periodically the coil current, stirring can be alternated.

In the case of Electro Slag Remelting (ESR), an alternating current is passed from the electrode to the water-cooled baseplate through a high-resistive calcium fluoride-based slag, thus generating Joule heating [2]. The energy is both transferred to the electrode for the melting and to the secondary ingot. Molten metal is produced in the form of droplets which fall and build up the secondary ingot, as shown in figure 1-b. Insulation from air and chemical refining, due to the presence of slag, improve the inclusional quality.

Remelted materials are special steels and nickel-based superalloys. Vacuum Arc Remelting also represents the final stage in the melting cycle of reactive metals, such as zirconium and titanium. The stra-

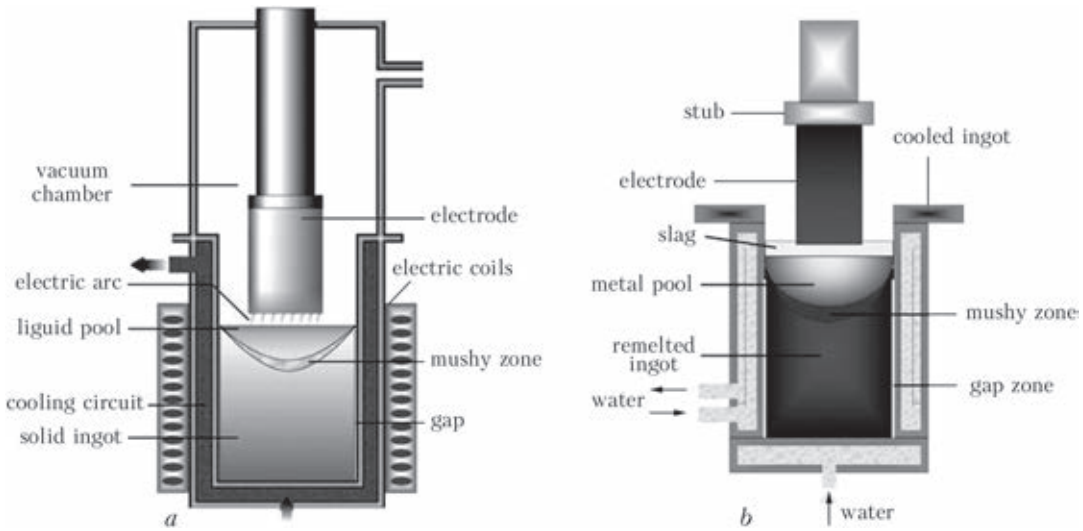

Figure 1. Schematic representation of (a) the VAR process, (b) the ESR process

tegic importance of these products and their very high added value make it essential to acquire a detailed understanding of the melting processes. Mathematical modelling is a valuable tool to enhance fundamental understanding, since it allows us to link operating parameters, such as the melting rate, ingot diameter or cooling conditions, to local solidification conditions, and thus to the ingot final quality. The work presented here is part of a program initiated some twenty years ago in Institut Jean Lamour to develop numerical software for simulating the remelting operations, and subsequently to help optimizing the processes. The first version of the numerical model SOLAR (which stands for SOLidification during Arc Remelting) was applied to the simulation of VAR for reactive metals [3]. Since then, the model has been constantly improved. In the beginning of the century, it was adapted for nickel-base superalloys and special steels.[4,5] More recently, a similar model has been developed for the ESR process [6]. The development started in 2004 with a basic hydrodynamic model of the slag, whose complexity was increased step by step. The last model has several common bases with the SOLAR code, since ESR and VAR are quite similar in terms of ingot growth and solidification.

A general description of both models (i.e. SOLAR and SOLECS, which stands for SOLar¬type Esr Complete Simulation) and their validation was part of a communication at the International Conference on Welding and Related Technologies into the Third Millenium, which was held in Kiev in 2008 [7]. Here, we will focus our attention on 3 recent studies aiming to develop some specific aspects of the behavior of actual remelting processes.

II. Current distribution during electroslag remelting

During the last years, several researches have been presented, aiming to simulate the whole process in a transient way, or discuss in more detail the electromagnetic fields in ESR [8–13]. Among these models, the simulation software SOLECS was developed at IJL, as stated in the Introduction. During the growth of the ESR ingot, the slag is in contact with the water-cooled mould, which is responsible for the formation of a layer of solidified slag at the interface. As the secondary ingot rises, this layer is partially remelted and crushed between the metal and crucible, resulting in a slag skin which acts as a thermal insulator and provides ESR ingots with a smooth lateral surface [2].

In the paper by Weber et al. [6], it was written that "*we assume that the solidified slag skin insulates electrically the slag and ingot from the mold. This assumption is particularly questionable and needs to be confirmed. Indeed, in some cases, the model predicts a discontinuous solid skin surrounding the slag cap, implying a possible electrical contact between liquid slag and mold*". While this strong assumption is made classically in the literature devoted to ESR simulation [14,15], it was sometimes claimed [16,17] that a certain amount of current is able to flow into the Cu crucible. This phenomenon could modify the thermohydrodynamic behaviour of the slag and liquid pool, hence influencing the solidification process. Therefore, the goal of our study is to quantify this phenomenon, and determine the impact of the solid layer thickness and electric conductivity of the solidified slag on the current distribution during electroslag remelting.

To reach the water cooled crucible and baseplate, the melting current supplied to the electrode and liquid slag can either flow in the ingot pool or directly through the solidified slag skin. The resulting current distribution depends on the electrical resistance of that phase, hence the solid slag conductivity and skin thickness. In this section, we present the computation of electromagnetic phenomena with a simplified geometry. The thickness of the solidified slag skin is assumed to be uniform and the assigned electrical conductivities are estimated values. The main input data are gathered in Table I.

The effects of the variations of two parameters (electrical conductivity and thickness of the solid slag layer, written with italic characters in Table I) on the current distribution and resulting Joule heating were studied. The electrical conductivity was allowed to vary in the range 10^{-3} — 400 $\Omega^{-1}\cdot m^{-1}$ (10^{-3} $\Omega^{-1}\cdot m^{-1}$ corresponds to a full insulation while 400 $\Omega^{-1}\cdot m^{-1}$ is the conductivity of the liquid slag). The thickness of the solidified slag skin was set to 4 or 6 mm. In the literature, the computed current distribution is most often represented by visualizing the magnitude of the current density phasor (i.e. the maximum value for each component of the current density), which classically leads to the observation of an important skin effect in the electrode and ingot [6,11,14,18]. Indeed, it is well known that the current distribution is related

Table I. Parameters used in the simulations

Melting current (maximum value)	10 kA
AC frequency	50 Hz
Electrode radius	26 cm
Mould external radius	30 cm
Mould thickness	2.5 cm
Electrode immersion depth	1 cm
Electrical conductivity of the metal	106 $\Omega^{-1}\cdot m^{-1}$
Electrical conductivity of the liquid slag	400 $\Omega^{-1}\cdot m^{-1}$
Electrical conductivity of the solid slag	10^{-3} — 400 $\Omega^{-1}\cdot m^{-1}$
Thickness of the solidified slag skin	4/6 mm

to the value of the skin depth into the different materials: if the latter is larger than the actual dimension of the domain, the current distribution is homogeneous, e.g. into the liquid slag. However, within this study, we chose to represent the instantaneous current distribution at a precise moment in the alternating period $t = 0$. In addition to the visualization of the skin effect, such a representation also highlights the local variation in the phase angle caused by the variation in the induced magnetic field into the metallic conductors, as it was shown by Li et al. [13].

The first step of the study consists in confirming that part of the melting current is likely to flow through the solidified slag layer and directly enter the mould. Figure 2 presents the computed results obtained either when the solid layer behaves as a perfect insulator (such behaviour is reached as soon as the electrical conductivity is lower or equal to 10^{-3} $\Omega^{-1}\cdot m^{-1}$) or when the electrical conductivity is set to 15 $\Omega^{-1}\cdot m^{-1}$. The solidified slag skin is supposed to be 4 mm thick. Clearly, when the electrical conductivity of the solid slag is set to 15 $\Omega^{-1}\cdot m^{-1}$, part of the current actually flows through the skin to reach the mould. The solidified slag layer does not act as a perfect electrical insulator and this modifies the current distribution in the system. Our result confirms some previous claims in the literature[16,17] and raises new questions regarding the consequences of such a loss of current on the process efficiency.

Figure 3 summarizes the effects of a variation in the electrical conductivity of the solid slag and in the thickness of the solidified slag layer: it represents the evolution of the total Joule heat generated according to both parameters. The electrical conductivity of the solid slag appears to be a crucial parameter of the process. This observation emphasizes the necessity to have access to actual measurements. The thickness of the solidified slag layer also influences the current distribution in the system. However, in the range of

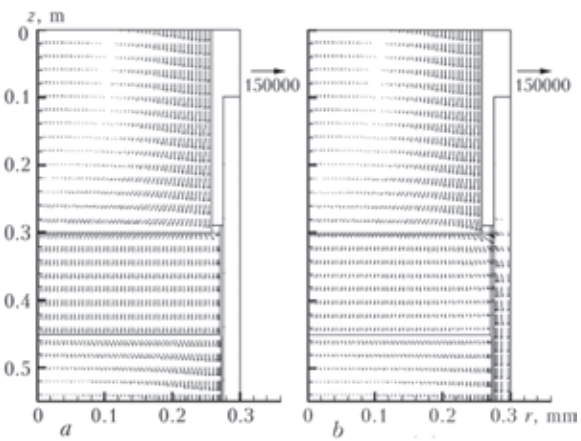

Figure 2. Current density distribution ($A\cdot m^{-2}$) computed with two values for the electrical conductivity of the solidified slag skin: 10^{-3} $\Omega^{-1}\cdot m^{-1}$ (a) and 15 $\Omega^{-1}\cdot m^{-1}$ (b)

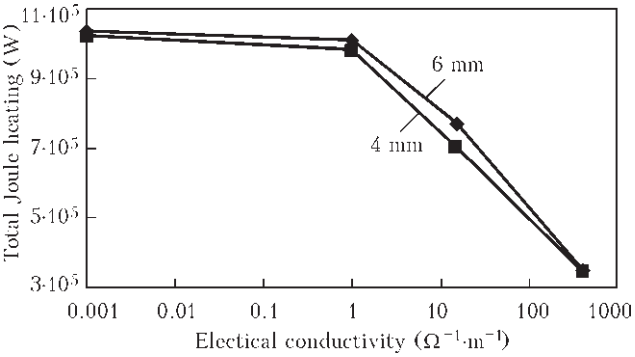

Figure 3. Evolution of the total resistive heating in the slag, according to the electrical conductivity and the thickness of the solidified slag skin

tested values, the impact of this factor remains of secondary importance.

In its present state, this model considered a uniform layer thickness along the slag/crucible interface. However, this parameter is liable to vary from a negligible value to few millimetres during a real remelting. To take into account this variation, as well as to assess the influence of the electrical current distribution on the ingot solidification, the next step of our study will consist in a full coupling of the model with a numerical simulation of the whole ESR process. Results obtained will be compared to actual experimental observation.

III. Ensemble arc motion during vacuum arc remelting

Knowledge of the electric arc behaviour in the VAR process is based on visualization studies performed first at Sandia National Laboratories [19] during the remelting of steel or Ni-based superalloy electrodes. Similar experiments have then been carried out by Chapelle et al. on Zr electrodes [20]. A conclusion from these observations is that the behaviour of the arc is similar to the diffuse mode of a vacuum arc created between cold solid electrodes. The arc consists of several dispersed clusters of cathode spots moving over the whole surface of the cathode. Such behaviour seems to imply that the total energy transferred from the arc to the cathode tip is distributed uniformly; in particular, no azimuthal direction is privileged, so an axisymmetric behaviour is expected at the macroscopic scale, consistent with the flatness of the cathode tip during full-scale melting.

However, it has been recently reported that the arc often does not behave axisymmetrically at the macroscopic scale. Based on measurements of the luminosity and magnetic field created by the arc [21, 22]. Ward et al. suggested that most of the time, the electrical centre of the arc was rotating in a time-averaged sense around the ingot centreline with a constant speed (period equals typically 20 to 40 s when a superalloy electrode melts under nominally diffuse conditions). Then it was assumed that the distribution of current flow and heat input followed the distribution

of this location and a part of the arc was assimilated to a loosely focused rotating spot, radially located away from the ingot centreline. A 3D model of the ingot pool, using this representation as a boundary condition, [23] enabled the authors to conclude that the hydrodynamic behaviour of the melt pool and ingot solidification process can be greatly influenced by such an ensemble arc macroscopic motion.

In order to confirm the previous statements, the dynamic behaviour of the arc in an industrial VAR furnace has been investigated. Two synchronized video cameras positioned in front of diametrically opposite viewing glasses on top of the furnace chamber were used to film the annulus gap between the electrode and crucible wall. Video images were recorded during the melt of a Zy2 ingot with various stirring conditions.

To help interpreting the recorded films, an image processing procedure similar to that proposed by Ward et al. [21] was developed. First, each film was split into a series of images. Then a 2 s moving average was applied to suppress high frequency fluctuations related to individual cathode spot behaviour and the sampling frequency was reduced to 5 frames/s. A given region of interest was extracted from each image and all the results were put side by side to build a temporal sequence (figure 4-a). Finally, the luminosity in the extracted region was quantified and a Fourier analysis was performed to determine the frequencies of fluctuations along the sequence.

An example of two sequences corresponding to diametrically opposite regions is illustrated in figure 4-b. A plot of the evolution of the luminosity for both sequences is also shown on the figure. The luminosity fluctuates quite regularly, with an alternation between very bright time periods and other time periods during which it is notably reduced. The fluctuations of luminosity in the two diametrically opposed regions are essentially in phase opposition. A frequency analysis indicates that these fluctuations involve several periods, with a dominating period of the order of 30 s, identical for the two cameras.

These fluctuations may be related to the arc behaviour. Indeed, it can reasonably be considered that the luminosity fluctuates as a consequence of the evolution of the spatial distribution of the arc, whose centre of gravity moves across the electrode surface with a period of about 30 s. This phenomenon was observed for all the melt conditions tested. The dominant period of the fluctuations was of the same order of magnitude for all melt conditions (including the conditions without any stirring). It seems in particular to be unconnected to the reversal period of the magnetic field. Thus, an ensemble motion of the arc seems to exist for all operating conditions and it appears to be relatively independent of the presence of an external axial magnetic field.

This work enables us to confirm the conclusions reached by Ward et al. [22] who reported a value of the time constant of the arc motion very similar to the one determined here. As discussed previously, the existence of a slow motion of the arc centre (with a time period of around 30 s) could have important implications for the modelling of the VAR process.

IV. Electromagnetic stirring and macrosegregation in var zirconium ingots

Despite the use of electromagnetic stirring, chemical heterogeneities develop in the mushy zone during the solidification stage. One of the main challenges for Zr and Ti producers is to master the VAR process in order to control the macrosegregation in remelted ingots. Macrosegregation results from the association of microsegregation and transport phenomena. The latter are primarily due to the flow in the liquid and mushy parts. It is now well established [24,25] that the hydrodynamics of the melt pool depends on

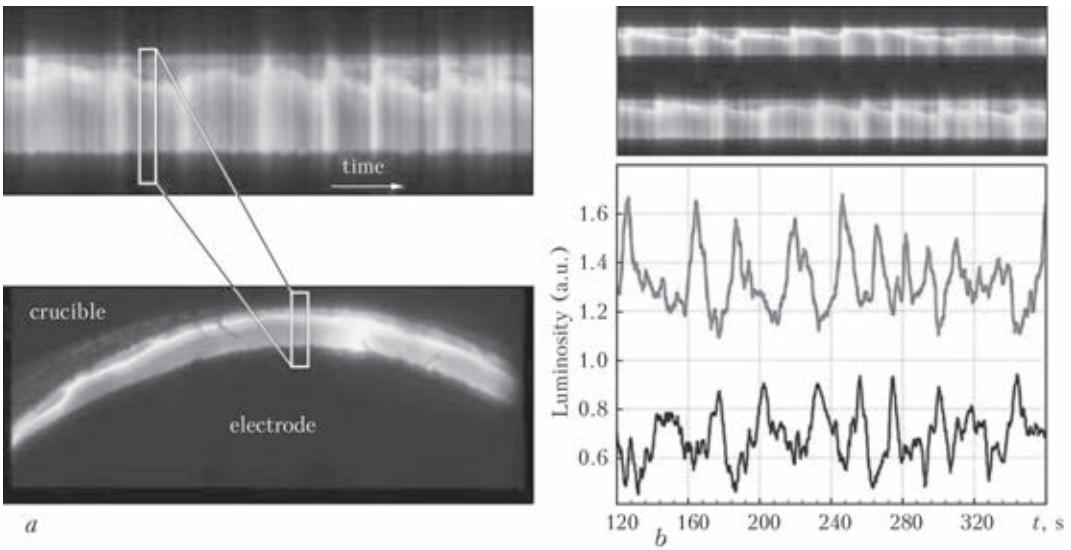

Figure 4-a. Temporal sequence used to study the fluctuations of luminosity above the ingot
Figure 4-b. Typical temporal sequences obtained for two diametrically opposite regions

the combined action of the followings: thermal and solutal buoyancy, self-induced electromagnetic force and the periodic centrifugal force caused by the angular movement generated by the stirring. The aim of this section is to investigate numerically the action of these forces on the macrosegregation of Zircaloy 4 VAR ingots.

In order to improve the description of the solidification and related macrosegregation, a multiscale model has been recently incorporated into SOLAR to simulate the solidification of multicomponent alloy VAR ingots. It is based on a volume-averaged Euler-Euler two phases formulation [26, 27]. At the macroscopic level, the permeability of the mushy zone is given by the Carman-Kozeny law, depending on a microstructure dimension typically of the order of the secondary dendrite arm spacing (SDAS). A macroscopic k-ε model that takes into account the actions of both the thermosolutal buoyancy and the influence of the solid phase in the mushy zone is used to simulate the turbulent nature of the flow. The phase change is treated locally at the microscopic level, either by assuming the lever rule or accounting for grain growth controlled by finite diffusion of alloy elements in both liquid and solid phases.

A Zy4 electrode was remelted in a production furnace. Two stirring sequences were successively applied: a strong alternated stirring followed by a weak continuous one. In addition, a continuous and strong stirring was temporarily used in order to mark several melt pools in the ingot. The recording of the actual operating process parameters provided input data for the model.

Thermosolutal buoyancy effects are simulated thanks to the Boussinesq approximation. Thermal and solutal expansion coefficients for Zr alloys are not available in the literature. Nevertheless, the thermal expansion coefficient β_T was estimated from data on pure liquid Zr. To investigate the influence of solutal convection caused by Sn concentration gradients (Sn is the major alloying element in Zy4), we have simulated 4 cases:

(a) $\beta_T = 0$, $\beta_S^{Sn} = 0$;

(b) $\beta_T > 0$, $\beta_S^{Sn} = 0$;

(c) $\beta_T > 0$, $\beta_S^{Sn} < 0$ and (d) $\beta_T > 0$, $\beta_S^{Sn} > 0$.

The positive value of the solutal expansion coefficient β_S^{Sn} (case d), was calculated from the volume additivity assumption. The other value (case c) was intentionally negative. Case a corresponds to the absence of all thermosolutal buoyancy, which means that the flow is only caused by the electromagnetic stirring.

For the four cases, the final maps of Fe segregation computed by the model are shown in figure 5. Because of the application of two successive stirring sequences, two main segregation patterns can be observed along the ingot height. In addition, we can

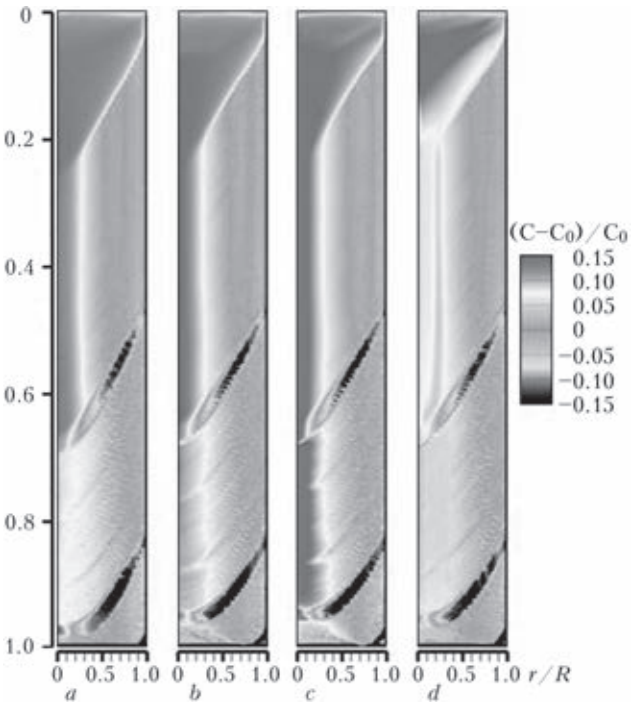

Figure 5. Maps of Fe segregation in the Zircaloy-4 VAR ingot for the 4 cases studied

see two inclined depleted bands caused by the pool markings. The enriched zone at the top of the ingot was caused by the solidification of the last melt pool. The average concentration of Fe in the liquid pool increases as the ingot grows because its partition coefficient is less than unity.

When thermosolutal buoyancy is not accounted for (case a), the model predicts an iron enrichment in the ingot central zone whatever the stirring employed. Actually, the centrifugal force due to the angular flow is predominant and generates a clockwise flow cell. Consequently, iron-enriched liquid accumulates at the bottom of the melt pool and in the mushy zone, causing a positive segregation near the axis. Alternated stirring causes a weaker radial macrosegregation than unidirectional stirring. For both stirring practices, accounting for thermal convection (case b) increases slightly the radial macrosegregation of the ingot central part, as thermal buoyancy strengthens the centrifugal force. In the mushy zone, the consequence is a more intensive circulation resulting into more transport of enriched liquid towards the centerline.

The effect of solutal convection on the centerline macrosegregation is visible on figures 5-c and 5-d. In case (c), radial segregation close to the centerline is notably amplified because all the volumetric forces cooperate. On the opposite, in case (d), the solutal buoyancy is counteracting and reverses the flow in the mushy zone at the bottom of the pool. The counterclockwise upward flow in the mushy zone reduces the segregation in the central region. When stirring is alternated (bottom half of the ingot), iron concentration is roughly uniform while a continuous stirring

(ingot top half) results in a positive segregation band located at r/R ~ 0.25 (R is the total radius of the ingot). This band forms due to the small counterclockwise flow loop induced by the solutal convection, which carries iron-rich liquid from the center to the outward radial direction.

The Fe segregation profiles predicted by the model clearly show that thermosolutal convection affects the macrosegregation only in the central region. In the upper part, chemical analyses show the Fe content rises continuously in the inner half of the ingot. Comparison with the model predictions reveals that such a behaviour is characteristic of case (d) where thermosolutal buoyancy is considered and $\beta_S^{Sn} > 0$. This shows that the upward flow driven by solutal buoyancy effects is partially responsible of the macrosegregation in Zy4 VAR ingots. In the outer part, where the centrifugal force is predominant, model and experimental results are in good agreement.

1. Choudhury, A. (1990) *Vacuum Metallurgy*. A.S.M. Int.
2. Hoyle, G. (1983) *Electroslag Processes — Principles and Practice*. Applied Science Publishers Ltd.
3. Jardy, A., Hans, S., Ablitzer, D. (1995) In: *Proc. MCWASP-VII*, TMS,1995, 205.
4. Quatravaux, T. et al. (2004) *J. of Materials Sci*., 39(**39**), 7183.
5. Jardy, A., Hans, S. (2006) In: *Proc. MCWASP-XI*, TMS, 2006, 953.
6. Weber, W. et al. (2009) *Metall. Transact. B*, **40B**, 271.
7. Jardy, A., Ablitzer, D. (2008) *The Paton Welding J*., **11**, 153.
8. Kelkar, K.M., Patankar, S.V., Mitchell, A. (2005) In: *Proc. LMPC*, 2005, ASM Int., 137.
9. Kharicha, A. et al. (2009) *In: Proc. LMPC*, 2009, TMS, 235.
10. Patel, A.D. (2011) *In: Proc. LMPC*, 2011, SF2M, 49.
11. Krane, M.J.M. et al. (2011) *In: Proc. LMPC*, 2011, SF2M, 65.
12. Kharicha, A. et al. (2012) CFD Modeling and Simulation of Materials Processing, Wiley/TMS, 139.
13. Li, B., Wang, F., Tsukihashi, F. (2012) *ISIJ Int*., **52**, 1289.
14. Jardy, A., Ablitzer, D., Wadier, J.F. (1991) *Metall. Transact. B*, **22B**, 111.
15. Hernandez-Morales, B., Mitchell, A. (1999) *Ironmaking and Steelmaking*, **26**, 423.
16. Mitchell, A. (2005) Materials Sci. and Engineering A, 413/414, 10.
17. Kharicha, A. et al. (2007) *In: Proc. LMPC*, 2007, SF2M, 113.
18. Dilawari, A.H., Szekely, J. (1977) *Metall. Transact. B*, **8B**, 227.
19. Zanner, F.J. (1979) *Ibid*, **10B**, 133.
20. Chapelle, P. et al. (2000) *High Temperature Materials Processing*, **4**, 493.
21. Ward, R.M., Jacobs, M.H. (2004) *J. of Materials Sci*., **39**, 7135.
22. Ward, R.M., Daniel, B., Siddall, R.J. (2005) *In: Proc. LMPC*, 2005, ASM Int., 49.
23. Yuan, L. et al. (2009) *Int. J. of Modern Physics B*, **23B**, 1584.
24. Jardy, A., Ablitzer, D. (2006) *Rare Met. Mat. Eng*., **35**, 119.
25. Venkatesh, V. et al. (2009) *J. Miner. Met. Mater. Soc*., **61**, 45.
26. Wang, C.Y., Beckermann, C. (1996) *Metall. Transact. A*, **27A**, 2754.
27. Zaloznik, M., Combeau, H. (2010) *Comput. Mater. Sci*., **48**, 1.

Received 09.04.2013